Thermal convection under external modulation of the driving force. II. Experiments

Guenter Ahlers
Department of Physics, University of California, Santa Barbara, California 93106

P. C. Hohenberg
AT&T Bell Laboratories, Murray Hill, New Jersey 07974

M. Lücke
Institut für Theoretische Physik, Universität des Saarlandes, D-6600 Saarbrücken, West Germany
(Received 7 August 1985)

Experimental data are presented on the temperature response of a Rayleigh-Bénard system to sinusoidal modulation of the heat current supplied to the lower plate near the onset of convection. Quantitative results are obtained for the average convective current as a function of the average Rayleigh number and of the amplitude and frequency of the modulation. Results are also presented on the temporal behavior of the response, above the convective threshold. The data are interpreted in terms of a previously proposed model which is a generalization of the Lorenz equations to periodic external driving. An important effect included in the model is the dynamic thermal mismatch between the sidewalls and the fluid which leads to an imperfect bifurcation between the conductive and convective states. As a result, the upward shift of the convective threshold caused by modulation in the ideal system is masked by the presence of sidewalls. In our model, this effect is controlled by a single adjustable parameter which turns out to agree in order of magnitude with previous experimental and theoretical estimates pertaining to a lower frequency range. The detailed comparison between experiment and theory shows good qualitative agreement, and some quantitative discrepancies in the parameter range explored. Suggestions are made for additional experiments to test a larger parameter range and in particular to minimize the sidewall effect in order to approximate the ideal threshold behavior more closely.

I. INTRODUCTION

This paper presents experimental results on the behavior of a Rayleigh-Bénard cell subjected to external temporal modulation of the heat input, and compares these results to the predictions of a model introduced in a previous paper[1] (hereafter referred to as I). Interest in the properties of externally modulated hydrodynamic systems of this type was originally stimulated by the experimental work of Donnelly *et al.*[2] on Couette-Taylor flow (see also Donnelly[3]). A considerable body of theoretical literature exists on this subject (see Davis,[4] Ahlers *et al.*,[1] and references therein), but the only experiments so far are those of Finucane and Kelly[5] whose results are primarily qualitative, and of Gollub and Benson[6] who operated far above the convective threshold where no quantitative theory exists.

The experiments reported here consist of measurements of the temperature response of a cylindrical Rayleigh-Bénard cell, whose lower plate is subjected to a sinusoidal heat current, and whose upper plate is kept at a fixed temperature. Just as in the absence of modulation, the occurrence of convection *at fixed external heat current* is signaled by a decrease in the average temperature difference between the lower and upper plate. This is because convection carries additional heat away from the lower plate and thus has a cooling effect. In the presence of modulation, however, there is yet another experimental signature of convection, which is absent for static heating: the temperature response to a *harmonic* heat current is itself *anharmonic* above the convective threshold. [Below threshold the conductive response should be purely harmonic if the experimental detection scheme is linear. This linearity was indeed verified to rather good accuracy in our experiments (see below).] The temporal harmonics which appear in the temperature response above the convective threshold contain detailed information about the convective state and their prediction is an important requirement for a successful theory.

Because our experimental setup involves external heating of the bottom plate only, rather than heating and/or cooling of both upper and lower plates or direct control of the temperature, there is an inherent limitation in the amplitude of the temperature modulation achievable in the apparatus. This maximum amplitude is controlled by changing the relative amplitude of the current modulation (which is at most unity) as well as the frequency; the amplitude of the temperature modulation turns out to be largest at low frequency for a fixed external current amplitude (a maximum relative temperature modulation of 50% was achieved in our work at a minimum dimensionless frequency $\omega = 3.2$).

In I we presented a theoretical model based on a mode truncation of the Oberbeck-Boussinesq equations of hydrodynamics.[7,8] Although this model involves drastic simplifications of the original equations, it reproduces quantitatively many central features of the full equations and has the additional virtue that its predictions can be

 ©1985 The American Physical Society

easily calculated and compared directly to the experimental data. The model, which is a generalization to the modulated case of the well known model of Lorenz,[9] consists of three coupled ordinary differential equations whose solution yields the convective current $j^{\text{conv}}(t)$ as a function of the time-dependent temperature difference (Rayleigh number) $r(t)$. The linear and nonlinear properties of the model near the convective threshold were studied in detail in I and were shown to agree well with the corresponding properties calculated directly from the Oberbeck-Boussinesq equations, in limits where the latter are available. For example, at low modulation amplitudes the convective threshold is shifted upward by modulation (stabilization of conduction) in a manner which is quantitatively reproduced by the Lorenz model for the ideal case of a laterally infinite system.

In the present paper we wish to use the Lorenz model to analyze real experiments which, of course, involve a finite cell with sidewalls. It has been shown earlier that near threshold the static effects of the finite geometry can be taken into account with reasonable accuracy by changing the values of the constant coefficients in the amplitude equation (see, e.g., Ahlers *et al.*[10]). Since the Lorenz model reduces to the amplitude equation in the static limit, a similar adjustment is expected to take into account the static effects of finite geometry for our problem. Of the remaining dynamic effects, it was shown by Cross *et al.*[11] for low frequencies, and by the present authors in I for the Lorenz model, that the most important effect is the appearance of horizontal currents. These currents are caused by the dynamic mismatch which results from the difference in thermal diffusivities between the fluid and the sidewall. They vanish in the static case, but in the presence of modulation they change the behavior compared to the laterally unbounded system. In particular, near the convective threshold of the ideal system the lateral currents can generate significant convective flow. Their effect was included in the Lorenz model in I by deriving the field $\xi(t)$ caused by the dynamic mismatch which forces rolls *parallel* to the sidewall. The strength of the sidewall forcing is measured by a (mismatch) parameter f, which was calculated within a model with stress-free horizontal boundaries by Cross *et al.*[11] The same parameter had been introduced earlier[10] to explain the onset time of convection when the Rayleigh number is raised from below to above R_c. In the present work the mismatch parameter f will be considered as an adjustable constant and its value determined by a particular modulation experiment. Once f has been fixed, the theory can be compared to experimental data with no further adjustable constants. This comparison between experiment and theory involves the average of the Rayleigh number as well as its time dependence, all considered as functions of the sinusoidally modulated external heat current.

An interesting effect observed in the experiment was an abrupt jump in average convective current as a function of the frequency (or amplitude) of the modulation. Moreover, at the transition point, anomalously long transients were observed in the dynamics. These observations have an explanation in terms of the Lorenz model in the presence of the forcing field. Indeed, the degeneracy between periodic states with opposite directions of rotation of the convection rolls, which exists in the ideal model, is lifted by the forcing field. Thus if the frequency (and with it the amplitude) of the temperature modulation are varied at fixed external heat current, a transition is observed in the model from a state of higher convective current to one of lower current. The similarity to the transition which occurs in the experiment lends detailed confirmation to the basic features of the model, in particular to the importance of the sidewall forcing term.

The comparison between experiment and theory leads to the following conclusions.

(i) The relation between the *averages* of the convective current and of the Rayleigh number, on the one hand, and the amplitude and frequency of the modulation, on the other hand, has been determined experimentally and agrees satisfactorily with the theory, over the range $3.2 \lesssim \omega \lesssim 20$, and $0.5 \gtrsim \Delta \gtrsim 0.1$, where ω is the modulation frequency in units of the vertical diffusion time, and Δ is the relative amplitude of the temperature variation.

(ii) The *temporal* behavior of the temperature response has been measured directly and that of the convective current has been determined indirectly. The harmonic content of both quantities was found to be in good accord with theoretical predictions.

(iii) Under the conditions of the experiments, the dynamical sidewall forcing introduces significant rounding of the convective transition and almost completely masks the upward threshold shift obtained from the equations for the ideal laterally infinite system.

(iv) The transition between two different periodic convective states observed when the modulation frequency is varied is in qualitative agreement with the predictions of the model. In one state, the convection is enhanced and in the other it is suppressed by the forcing.

The favorable comparison mentioned earlier between the Lorenz model and results obtained from the full Oberbeck-Boussinesq equations in special cases depends on the assumption that the basic flow pattern is not changed by modulation. This assumption was recently shown by Roppo *et al.*[12] to be false for an ideal laterally infinite system. Instead, these authors found that modulation near the convective onset leads to a subcritical bifurcation to a hexagonal pattern. However, this phenomenon seems to be quite sensitive to sidewall forcing. Indeed, a flow visualization experiment by Steinberg *et al.*[13] has shown that sidewall forcing favors a roll pattern, so that the hexagonal solution is suppressed.

It should also be noted that the chaotic features of the solutions of the model, which have been studied theoretically by many authors since the original work of Lorenz,[9] are not relevant to our investigation since they occur far above the convective threshold in a region which we did not investigate experimentally. In any case, the Lorenz truncation cannot be expected to reflect the behavior of a real fluid in that parameter range.

In Sec. II we introduce notations and definitions. Section III describes the experimental apparatus and method, and Sec. IV discusses the method of data analysis used for both the time averages and the time dependence. The results are then presented in Sec. V, and Sec. VI concludes

with a brief discussion of future experimental work. Preliminary reports of the present results were published earlier.[14,15]

II. NOTATION

In this section we define the various currents and temperature response functions to be used later. (Unless otherwise stated, the notation is the same as that of our previous work[1,15] but we repeat the definitions here for completeness.) Throughout most of the paper we use dimensionless units in which lengths, times, temperatures, and pressures are scaled by d, d^2/κ, $\kappa\nu/\alpha g d^3$, and $\rho\kappa^2/d^2$, respectively. Here d is the plate separation, κ the thermal diffusivity of the fluid, ν its kinematic viscosity, α its thermal expansion coefficient, ρ its density, and g the acceleration of gravity.

Let the dimensionless temperatures of the upper and lower plates be $T^u(t)$ and $T^l(t)$, respectively (t is the time). Then the time-dependent Rayleigh number is

$$R(t)=T^l(t)-T^u(t) . \tag{2.1}$$

In the absence of time dependence and for a Boussinesq fluid, $R(t)$ reduces to the usual static Rayleigh number whose critical value is $R_c^{\rm stat}$. The basic experimental input is the vertical heat current $J(t)$ applied to the lower plate. We define a reduced current

$$j(t)=J(t)/R_c^{\rm stat} \tag{2.2}$$

by dividing $J(t)$ by the current $J_c^{\rm stat}=R_c^{\rm stat}$ at criticality in the absence of time dependence. Similarly, the reduced Rayleigh number is given by

$$r(t)=R(t)/R_c^{\rm stat}=[T^l(t)-T^u(t)]/\Delta T_c^{\rm stat} . \tag{2.3}$$

The total current $j(t)$ consists of a conductive part and a convective part written as

$$j(t)=j^{\rm cond}(t)+j^{\rm conv}(t) . \tag{2.4}$$

In the present experiments the temperature T^u was constant. We used purely sinusoidal modulation of the input current

$$j(t)=j_0+\hat{j}_1\sin(\omega t) \tag{2.5}$$

(in Ref. 15 the quantity $\hat{j}_1$ was denoted a). We shall study the response of the system to the modulation (2.5) in a parameter region where in steady state all response functions are periodic with the period $2\pi/\omega$ of the driving. It is then convenient to use the Fourier decomposition

$$A(t)=\sum_{\nu=-\infty}^{\infty} A_\nu\exp(-i\omega\nu t) , \tag{2.6}$$

where $A(t)$ is any of the *real* periodic functions appearing in this work [e.g., $r(t)$, $j^{\rm conv}(t)$, $j^{\rm cond}(t)$, etc.]. Note that A_0 is the time average of $A(t)$ and reality of $A(t)$ requires

$$A_\nu=A^*_{-\nu} . \tag{2.7}$$

For example, the sinusoidal input current (2.5) has average j_0 and coefficients

$$j_1=j^*_{-1}=\hat{ij}_1/2,\quad j_\nu=0,\quad |\nu|\geq 2 . \tag{2.8}$$

As discussed in the Introduction, a sinusoidal input current induces a temperature difference

$$r(t)=r_0+2\,{\rm Re}(r_1e^{-i\omega t})+\cdots \tag{2.9}$$

where the ellipsis represents higher-harmonic terms. If one ignores their contribution, which is in general quite small, one may write $r(t)$ in the form

$$r(t)=r_0{\rm Re}(1+\Delta e^{-i\omega t}) . \tag{2.10}$$

This notation was introduced in I, and will be used here also occasionally. Then

$$\Delta=2r_1/r_0 \tag{2.11}$$

determines the relative amplitude of the temperature variation around the mean r_0. In the purely conductive state ($j^{\rm conv}=0$), we expect a linear relation between the heat current and the temperature which may be expressed in terms of the transfer function $\mathscr{P}(\omega\nu)$ defined by

$$j_\nu^{\rm cond}=r_\nu/\mathscr{P}(\omega\nu) \tag{2.12}$$

(see Appendix B). In the presence of convection, the conductive part of the current is still related to the Rayleigh number by Eq. (2.12) with the same function $\mathscr{P}(\omega\nu)$ as in the conductive state (but of course a different r_ν). Quite generally, at zero frequency, we have $\mathscr{P}(0)=1$, so the average Rayleigh number is equal to the average conductive current, i.e.,

$$j_0^{\rm cond}=r_0=j_0-j_0^{\rm conv} . \tag{2.13}$$

III. EXPERIMENTAL APPARATUS AND METHOD

A. System properties

The apparatus used in this work was described in detail by Behringer and Ahlers,[16] hereafter referred to as BA. For the present experiments, we used cell A of that reference. It was $d=0.265$ cm high, had an aspect ratio $D/2d=4.72$ (D is the diameter), and was of cylindrical symmetry. The fluid was liquid normal ^{4}He, and most experiments were carried out at saturated vapor pressure and at a top temperature of 2.1841 K, where the Prandtl number is $\sigma=0.78$. Temperatures are measured on the 1958 ^{4}He vapor-pressure scale of temperatures.[17] At that temperature and pressure, the thermal conductivity K and the thermal diffusivity κ of the fluid were 1607 erg/s cm K and 2.26×10^{-4} cm^2/s, respectively. The corresponding vertical thermal diffusion time $t_V\equiv d^2/\kappa$ was 311 s. The temperature difference at the static convective onset was 5.0×10^{-4} K. For this case, the Oberbeck-Boussinesq equations provide an accurate description of the real system.[16,18]

The cell walls were made of stainless steel, and, in the absence of convection, they carried about 12% of the total heat flux. The wall thickness was $t_w=0.058$ (in units of d). The ratio of the fluid conductivity to the wall conductivity was $\lambda_2=0.17$, and the corresponding ratio of the thermal diffusivities was $\lambda_1=6\times10^{-4}$.

B. Procedure

In order to compare the data with the model described in Sec. IV A below, it is necessary to know the initial slope $1/\bar{g}$ of the Nusselt number under conditions of static heating ($\hat{j}_1=0$). Measurements by BA revealed that there exist two different convective states, corresponding to $1/\bar{g}=0.56$ and 0.83 (see Fig. 13 of BA). The state with $1/\bar{g}=0.56$ was formed initially upon passing through the convective threshold, but under static conditions it was unstable and decayed to the other state for all $r_0>1$. We found that modulation stabilized this state for $1.0\leq r_0\lesssim 1.1$. For larger r_0, it was unstable even in the presence of modulation with the amplitudes and frequencies employed in this work. In the analysis of the data, we shall use whichever value of $\bar{g}$ is appropriate to the particular value of r_0 in each run [the choice is quite clear on the basis of the experimental segments without modulation (see below)].

The modulation experiments were conducted by applying a heat current $j(t)$ to the cell bottom while holding constant the temperature T^u at the top, and by measuring the cell bottom temperature $T^l(t)$. The current $j(t)$ was generated by a resistive heater and a voltage produced by a computer and digital-to-analog converter (DAC). During periodic modulation, its value was updated 256 times per cycle. The temperature $T^l(t)$ was determined by measuring the unbalance of an ac germanium-resistance thermometer bridge using a 12-bit analog-to-digital converter (ADC) and the computer (for details, see BA). Measurements of $T^l(t)$ were made 32 times per modulation cycle. As mentioned above, we used purely sinusoidal modulation of $j(t)$, given by Eq. (2.5). Note that this choice fixes the time origin of the measurement sequence and thus determines the phase of the $T^l(t)$ measurements.

An experimental measurement sequence usually consisted of several segments with different frequencies ω but the same amplitudes j_0 and $\hat{j}_1$. A few sequences at constant ω with segments of different j_0 were also obtained. Each segment consisted of n cycles (typically $n=40$) followed by an equally long time period (i.e., $2\pi n/\omega$) with the same j_0 but with $\hat{j}_1=0$ (i.e., the same mean current but no modulation). The response of the temperature difference to the applied current is shown in Fig. 1 for part of a sequence. Concentrating on the data for $\omega=9.8$, one may note that there are transients during the early cycles. The large peak associated with the first cycle is attributable to the fast transients inherent in the establishment of the periodically time-dependent conduction temperature profile, and the lesser effect noticeable during the first five cycles is associated with the slower process of the convecting state adjusting to the modulation. That same longer time scale is noticeable near the right edge of the figure, where $\hat{j}_1=0$ and where the convecting state once more undergoes adjustment. Data during these transient cycles were discarded.

In Figs. 2(a)–2(c), we show one cycle of the applied current, and one cycle of the steady-state temperature response to that current at two different frequencies. The large phase shift of $r(t)$ relative to $j(t)$ is apparent and attributable primarily to the conductive response. Likewise, the amplitude $|r_1|$ of r can be explained largely in terms of $j_1^{\rm cond}$ and $\mathscr{P}(\omega)$ [Eq. (2.12)]. Although harmonic distortion is not very obvious on the scale of Fig. 2, the data contain significant information about the convective contribution to $r(t)$ which will have to be extracted by an appropriate analysis (see Sec. IV below).

In the data analysis, the time origin for each segment

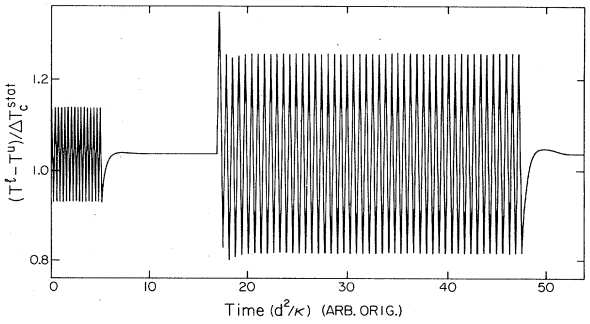

FIG. 1. Response of the vertical temperature difference across the cell (divided by the critical value at onset of convection under static heating) to variation of the heat current applied to the bottom plate as a function of time. In the two oscillatory segments of the figure the current was sinusoidally modulated with the same amplitude $\hat{j}_1=1.00$ but different frequencies ($\omega=19.6$ and 9.8, respectively) around a mean value $j_0=1.06$. Transients between static and periodic response (or vice versa) of the temperature are caused by switching the current modulation on (and off), keeping j_0 unaltered.

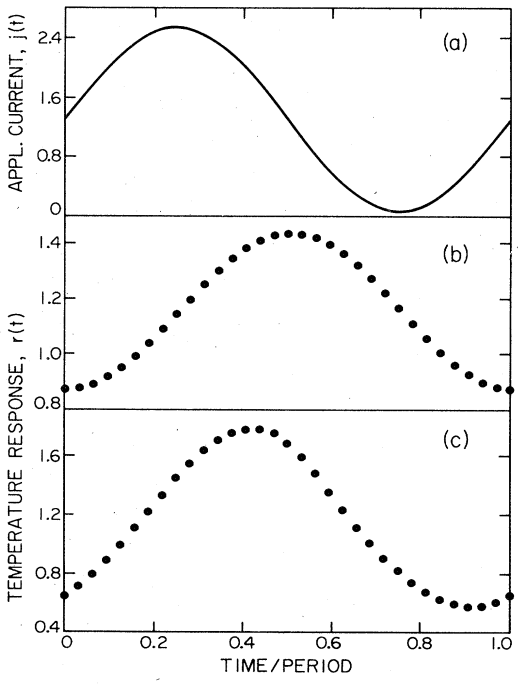

FIG. 2. (a) Sinusoidally modulated heat current $j(t)=1.30+1.23\sin(\omega t)$ and steady-state periodic temperature response $r(t)$ for modulation frequencies (b) $\omega=9.79$ and (c) $\omega=3.91$ as a function of time during one period of the modulation.

was taken at the beginning of the ninth modulation cycle, i.e., the first eight cycles were discarded to avoid transient effects. This typically left 32 cycles, or 1024 data points, for analysis. Measurements of T^l with zero applied current were obtained only before and after the complete sequence consisting of typically six segments. Since a sequence often extended over several days, the results for $T^l(t)-T^u$ are subject to small systematic errors (a few tenths of a percent of $\Delta T_c^{\rm stat}$) associated with long-term experimental drifts. For this reason, the most accurate information about the effect of modulation upon the mean value r_0 of $r(t)$ is obtained by comparing the subsegments with $\hat{j}_1=0$ and $\hat{j}_1>0$ within the same segment. The Fourier components of $r(t)$ are, of course, not influenced significantly by the small long-term drift.

It should be remarked that our experimental procedure implies that $j(t)\geq 0$ for all t; i.e., the bottom is always heated and never cooled except by conduction through the sample and sidewalls. This restricts the amplitudes $|r_1|$ of $r(t)$ to values less than one-half the mean value $r_0/2$ of r. The largest possible temperature variation, which is obtained for $\hat{j}_1=j_0$, is given by $|r_1|=\frac{1}{2}|\mathscr{P}(\omega)\hat{j}_1|$, where $\mathscr{P}(\omega)$ is considerably less than unity for our modulation frequencies (cf. Fig. 4 below). As discussed in I, many interesting phenomena due to modulation occur at larger amplitudes and thus are not within the scope of the present experimental investigation.

C. Properties of the conductive state

Since comparison of our experimental data with the theoretical model of I involves identifying rather small deviations from linear relations between currents and temperature differences, it is important to check that the measuring apparatus does not introduce spurious nonlinear effects. This can be done most conveniently in the conductive state, since there the relation between j_ν and r_ν [see Eq. (2.12)] should be linear. Thus a set of experiments was carried out at a top temperature of 2.1794 K where the critical temperature difference is relatively large because the expansion coefficient of liquid ^{4}He at vapor pressure is small. In that case, a steady heat current $j=j_0=0.678$ was used and produced a temperature difference about equal to the critical temperature difference at the normal operating temperature of 2.1871 K. When a *modulated* current $j(t)$, with $\hat{j}_1=0.630$, $j_0=0.678$, was used instead, essentially no convection occurred. This is demonstrated by considering the ratio $r_0/r_{\rm stat}\equiv r_0(\hat{j}_1\neq 0)/r_0(\hat{j}_1=0)$ of the average Rayleigh number with and without modulation, at fixed average current j_0. The data are displayed in the second column of Table I, and they show that modulation has altered r_0 by no more than 0.2%. As discussed in Sec. III B, an effect of this size may be attributable to long-term drifts of the apparatus rather than to convection. If the modulation had induced significant convection, then r_0 would have been reduced, according to Eq. (2.13), by a larger amount.

We searched further for any undesirable nonlinear effects in this run with $j_0<1$ by examining the Fourier coefficients of $r(t)$. The third and fourth columns of Table I contain $|r_1|$ and $|r_2|$ (note that $r_0=j_0$ for $j_0=0.678<1$). The values of $|r_1|$ are established in direct linear response to the driving current with amplitude $\hat{j}_1$ [see Eq. (2.12)]. However, any significant contribution to r from r_2 would be indicative of undesirable nonlinear effects in the experiment. The values found for $|r_2|$ are only about 0.2% of the corresponding $|r_1|$. Higher harmonics were not detectable at all. Thus, spurious nonlinear effects of experimental origin are quite small.

IV. DATA-ANALYSIS METHODS

A. The Lorenz model

We shall analyze our data using the Lorenz model introduced in I, which consists of three nonlinear equations for the variables $x(t)$ and $y(t)$ representing the lowest velocity and temperature modes, and for the variable $z(t)$ representing the *spatial average* of the temperature in the horizontal plane. In deriving the Lorenz model in I, we used the usual decomposition into spatial Fourier components and retained a single horizontal wave number for the velocity and temperature modes $x(t)$ and $y(t)$. Clearly, this corresponds to a grossly oversimplified description for a finite system, especially one with cylindrical symmetry as is the case with the present experimental cell. On the other hand, near threshold and in the absence of modulation, the Lorenz model reduces to an amplitude equation which is a generally valid description even for finite systems (see Ahlers *et al.*[10] and Cross *et al.*[11]). The most important effects of geometry are taken into account by a change in the constants appearing in the amplitude equation, primarily in the coefficient $\bar{g}$ which relates the convective current or Nusselt number to the Rayleigh number. In applying the Lorenz model to our finite cylindrical system, we shall similarly consider $x(t)$ and $y(t)$ to be the amplitudes of the lowest spatial modes of the velocity and temperature, respectively, in the finite cell, and adjust the constant $\bar{g}$ to give the correct Nusselt number near threshold in the absence of modulation. Thus, it is only the *difference* between the behavior with and without modulation which our theory attempts to calculate, and it is hoped that most of the effects of finite geometry will be unimportant in evaluating this difference. One effect which we do take into account, however, is the forcing of convection due to the time-dependent sidewall heating, since this effect vanishes in the static case and leads to convection even below the ideal threshold in the presence of modulation.

The equations for our model are [see Eqs. (2.8), (2.14), (2.32), and (5.2) of I]

$$\tau_1\frac{dx}{dt}=-\tilde{\sigma}[x(t)-y(t)]+\tilde{\sigma}\xi(t)\ , \tag{4.1a}$$

$$\tau_1\frac{dy}{dt}=-y(t)+[\tilde{r}(t)-z(t)]x(t)\ , \tag{4.1b}$$

$$\tau_1\frac{dz}{dt}=-b[z(t)-x(t)y(t)]\ , \tag{4.1c}$$

$$\tau_1=\tau_1^r=(2\pi^2)^{-1}\ , \tag{4.1d}$$

$$\tilde{\sigma}=\tilde{\sigma}_r=27\sigma/14\ , \tag{4.1e}$$

$$b=b_r=2\ , \tag{4.1f}$$

$$\tilde{r}_v=r_v\frac{9\pi^4 q_v}{2\tan(q_v/2)(\pi^2-q_v^2)(9\pi^2-q_v^2)}\ , \tag{4.1g}$$

$$q_v=(i\omega v)^{1/2}\ , \tag{4.1h}$$

where σ is the Prandtl number of the fluid, and as explained in I, the difference between $\tilde{r}_v$ and r_v [Eq. (4.1g)] arises because the conduction profile is not a linear function of the vertical coordinate x_3 when the temperature across the cell is time dependent.

Within the model the convective current is given by

$$j_{\rm conv}(t)=\bar{g}^{-1}z(t)\ , \tag{4.1i}$$

where $\bar{g}$ is the constant relating the Nusselt number $N\equiv j_0/j_0^{\rm cond}$ to the Rayleigh number in the absence of modulation ($\hat{j}_1=0$, $r=r_0$, $j^{\rm conv}=j_0^{\rm conv}$). For this case we have to first order in r_0-1,

$$j_0^{\rm conv}/r_0=N-1=\bar{g}^{-1}(r_0-1)=\bar{g}^{-1}z_0\ . \tag{4.2}$$

In Eqs. (2.31b) and (2.32d) of I the exact and approximate theoretical values $\bar{g}=g_r$ for a laterally infinite system with rigid top and bottom plates were quoted, but we shall use the experimental values for $\bar{g}$ obtained in the absence of modulation by BA (see Sec. III B above). The difference between the experimental values and the value $g_r=0.707$ resulting from Eq. (2.31b) of I (for $\sigma=0.78$) is attributable to the static effect of sidewalls which change the flow pattern from the one assumed in I, i.e., parallel rolls at the critical wave number.

The sidewall forcing function $\xi(t)$ in Eq. (4.1a) has Fourier coefficients given by [see Eqs. (5.3) and (5.4) of I]

$$\xi_v=-i\omega v f r_v\psi(\omega v)\ , \tag{4.3}$$

where the function ψ is such that $\psi(0)=1$ and $\psi(\pm\infty)=0$, and the mismatch parameter f can either be calculated approximately[11] or treated as an adjustable parameter which is fitted to experiment.[10] In Appendix A we quote the results for f and ψ obtained in I from a calculation of sidewall effects within the Lorenz truncation. For analyzing the present experimental data we shall treat f as an adjustable parameter and use the theoretical values for ψ. The parameter f is related to $\bar{f}^1$ of Refs. 10 and 11 by $f=\tau_1(1+\tilde{\sigma}^{-1})\bar{g}^{1/2}\bar{f}^1$.

B. Spectral analysis

The comparison between the experimental data and solutions of the model is best accomplished with the aid of spectral analysis. The Fourier coefficients of the measured $r(t)$ and of the calculated $z(t)$ were obtained with a fast Fourier transform method, employing 32 data points per cycle. The time series to be Fourier transformed consisted of 32 cycles. Although the series were of finite length, the Fourier spectra nevertheless consist of sharp lines at the basic frequency ω and its harmonics. This is so because the time intervals Δt between the data points were chosen to be commensurate with the period, i.e., $32\Delta t=2\pi/\omega$. As an example we show in Fig. 3 the power spectrum of $r(t)$ (which is proportional to the square of the absolute value of the Fourier coefficients) for two different driving frequencies $\omega=9.79$ and 3.91, but with the same j_0 and $\hat{j}_1$ in Eq. (2.5). For $\omega=9.79$, the harmonic generation at $2\omega=19.58$, which is due to convection, is quite weak, though it is significantly larger than the value obtained in the absence of convection (see Table I). At the lower driving frequency in Fig. 3, $\omega=3.91$, there are many harmonics, and, even at a frequency of 19.58, which corresponds to the fourth harmonic of 3.91, the power is greater than it was at the first harmonic of $\omega=9.79$. Thus, it is seen that at constant j_0 and $\hat{j}_1$ the lower driving frequency [which yields a larger amplitude of $r(t)$] clearly influences the convecting state more strongly.

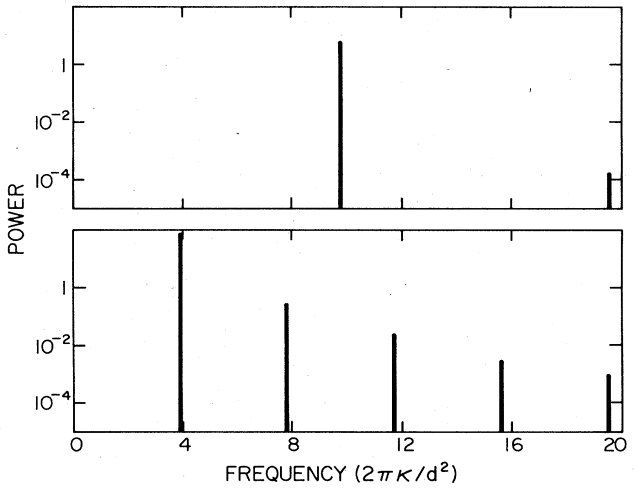

FIG. 3. Power spectra of the temperature response $r(t)$ shown in Figs. 2(b) and 2(c). Upper figure is for $\omega=9.79$ and the lower figure for $\omega=3.91$.

C. The conductive transfer function $\mathscr{P}(\omega)$

Both the conductive current and the convective current can be determined from the experimentally measured $r(t)$ if the transfer function $\mathscr{P}(\omega)$ of the system is known. The evaluation of $j_v^{\rm cond}=r_v/\mathscr{P}(\omega v)$ [Eq. (2.12)] also gives $j^{\rm conv}(t)=j(t)-j^{\rm cond}(t)$ since the total current $j(t)$ is externally controlled in our experiments.

For idealized geometries the function $\mathscr{P}$ can be calcu-

TABLE I. Magnitudes of Fourier coefficients of the temperature response in the conductive regime. Driving current was sinusoidally modulated (with amplitude $\hat{j}_1=0.630$) around a subcritical mean ($j_0=0.678$). Second column shows that modulation has altered the mean reduced Rayleigh number by less than 0.2% compared to the static driving ($\hat{j}_1=0$).

ω	$r_0/r_{\rm stat}$	$\lvert r_1\rvert$	$10^3\lvert r_2\rvert$
9.77	0.9981	0.078	0.16
6.51	0.9984	0.105	0.25
4.88	0.9987	0.130	0.35
3.91	0.9994	0.154	0.47

lated. For example, in the absence of lateral boundaries, and for a lower plate with nonzero heat capacity and a conductivity which is much larger than that of the fluid, we have

$$\mathscr{P}(\omega\nu)=\frac{\tan(q_\nu)/q_\nu}{1-\lambda_3^2 q_\nu \tan(q_\nu)} . \tag{4.4}$$

Here $q_\nu=(i\omega\nu)^{1/2}$ and λ_3^2 is the ratio of thermal masses of the lower plate and the fluid. A derivation of this equation is given in Appendix B of this paper.

For our experimental system, Eq. (4.4) is not sufficiently accurate, and it was necessary to measure $\mathscr{P}(\omega)$ experimentally. This was done by driving the system at various frequencies ω under conditions where convection was absent. From the driving current $j(t)=j^{\rm cond}(t)$, and the Fourier transform of the response $r(t)$, the transfer function $\mathscr{P}(\omega)$ was determined. Our experimental results for the absolute value $|\mathscr{P}|$ and the phase $\phi_{\mathscr{P}}$ are compared with Eq. (4.4) in Figs. 4(a) and 4(b). The absolute value of $\mathscr{P}$ agrees well with the data if $\lambda_3=0.35$ is used, but the phase does not fit well for any value of λ_3. Introducing a finite ratio of the conductivity of the fluid to that of the lower plate does not improve the fit of the phase data, and in any event a finite ratio is unrealistic in view of the large conductivity of copper of which the lower plate was made. Presumably, the deviation of $\phi_{\mathscr{P}}$ from the prediction in Eq. (4.4) is due to the lateral boundaries which make the heat-flow problem two dimensional. In any case, for comparison of the data with the model, we used the experimental values of $\mathscr{P}$ to determine $j_\nu^{\rm cond}$ from r_ν.

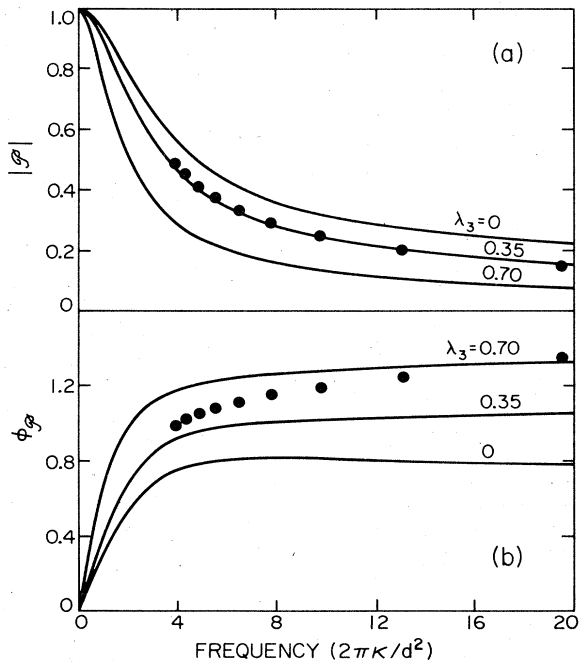

FIG. 4. Modulus $|\mathscr{P}(\omega)|$ (a) and phase $\phi_{\mathscr{P}}$ (b) of the conductive transfer function [defined by $\mathscr{P}(\omega\nu)=r_\nu/j_\nu^{\rm cond}$] vs frequency ω. Lines represent the analytical result (4.4) obtained for an idealized system (cf. Sec. IV C and Appendix B) with three different ratios λ_3^2 of thermal masses of the lower plate and the fluid. Solid circles show experimentally determined values for our system. See Sec. IV C for more details.

D. Inversion of the model

The solution of the differential equations (4.1) defining our model gives the convective current $j^{\rm conv}(t)=z(t)/\bar{g}$ as a function of $r(t)$, i.e., $z_\nu=z_\nu(\{r_\mu\})$. On the other hand, in the experiments, $r(t)$ was measured for given total current $j(t)$. In order to compare the measurements with our model, we inverted the relations

$$j_{\rm conv}(t)=j(t)-j_{\rm cond}(t) , \tag{4.5a}$$

$$\bar{g}^{-1}z_\nu(\{r_\mu\})=j_\nu-r_\nu/\mathscr{P}(\omega\nu) \tag{4.5b}$$

to find r_ν and with it $r(t)$ as a function of $j(t)$. The implicit equations (4.5) for r_ν were solved numerically by an iteration method described in detail in Appendix C. The essence of this procedure is to start with a trial set $\{r_\nu\}$ and evaluate the convective current $z_\nu/\bar{g}$ from the model equations (4.1). From this a revised set of r_ν's can be calculated, given by $r'_\nu=(j_\nu-z_\nu/\bar{g})\mathscr{P}(\omega\nu)$, as follows from (4.5b). The procedure is then repeated until r_ν ceases to change with each iteration. Note that this solution method involves repeated integration of the differential equations (4.1) to find a stationary periodic state.

V. RESULTS

The results we present below consist mostly of steady-state data for the temperature response $r(t)$, with various values of the applied current $j(t)$, Eq. (2.5), i.e., with different values of j_0, $\hat{j}_1$, and ω. Since in steady state the response is a periodic function of time, we can summarize the results by discussing the average value r_0, on the one hand (part A), and the strength of various harmonics of r (part B), on the other. As explained earlier, comparison with the Lorenz model of Sec. IV involves the single adjustable parameter f in Eq. (4.3), which measures the strength of the sidewall forcing field. This parameter affects the results most strongly near the convective threshold, so we first discuss data in this region and then turn to the behavior above threshold.

A. Mean values

1. *Field effects near the convective threshold*

The mean value $j_0^{\rm conv}$ of the convective current is obtained from the imposed mean current j_0 and the measured Rayleigh number r_0 via Eq. (2.13). We determined the mismatch parameter f of Eq. (4.3) by fitting the Lorenz model to experimental data near the ideal threshold, i.e., with j_0 close to unity. This is where the effect of the forcing on the convective heat transport is largest so that f can be determined most accurately. Measurements were made for several closely spaced values of j_0, with $\hat{j}_1=j_0-0.066$. The fit yielded $f=0.005$ for $\omega=3.26$. [Note that only the absolute value of f is significant; its sign is arbitrary since the model (4.1) is invariant under the transformation $(x,y,f)\rightarrow-(x,y,f)$.] The value $f=0.005$, which will be retained throughout the

remainder of the analysis, corresponds to $\bar{f}^{1}=0.044$, and is about a factor of 3 larger than that found earlier from a fit to onset time experiments by Ahlers *et al.*[10] and from the model calculation by Cross *et al.*[11] (the two earlier determinations agreed with each other). In view of the rather large difference between the frequency ranges of the present work and the earlier investigations, we do not expect better than order of magnitude agreement in the values obtained for f in the two cases.

The data on the average convective current $j_0^{\rm conv}$ versus the average reduced Rayleigh number r_0 are shown in Fig. 5 for the two frequencies $\omega=3.26$ (solid circles) and $\omega=6.51$ (open circles), both with $\hat{j}_1=j_0-0.066$ and j_0 varied in small steps. It is important to note that for the same values of j_0 and $\hat{j}_1$ the temperature response $r(t)$ in the presence of convection is quite different for the two frequencies shown. For the mean values, we have $r_0\simeq j_0$ in both cases, but r_1 depends upon ω. In particular, at the lower frequency ($\omega=3.26$) $\Delta\cong 0.50$, and at the higher frequency $\Delta\cong 0.29$. Thus an effective method of changing the amplitude Δ of the *temperature* variation in the present experiment is to change the frequency of the applied sinusoidal current.

In Fig. 5 we also show as solid lines the predictions of the Lorenz model for the conditions of the experiment. Overall agreement with the $\omega=3.26$ data is good because those data were used to fix the value of f. Nonetheless, the detailed agreement in the r_0 dependence between model and data is significant. The $\omega=6.51$ data show only a very small $j_0^{\rm conv}$, but within the experimental uncertainty of about 10^{-3} in both r_0 and $j_0^{\rm conv}$ they also agree with the model. The strong dependence of $j_0^{\rm conv}$ on the temperature amplitude Δ and the frequency ω is consistently reflected in both the model (solid lines) and the data. The perfect bifurcation of the unmodulated ideal system is shown in Fig. 5 as a dotted line. The perfect bifurcations in the modulated ideal system ($f=0$), which exhibit the stabilization of the conductive state by modulation, are shown as dashed lines. It is clear that the sidewall forcing represented by f has a strong effect upon $j_0^{\rm conv}$. For both of the experimental frequencies, the field f largely masks the stabilization effects inherent in the ideal model near threshold.

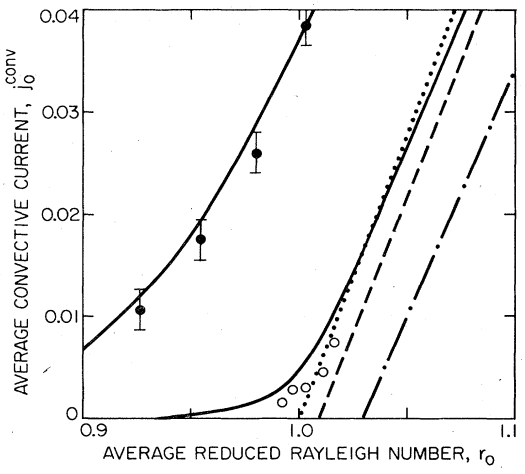

FIG. 5. Average convective current $j_0^{\rm conv}$ vs average reduced Rayleigh number r_0 resulting from a total heat current $j(t)=j_0+\hat{j}_1\sin(\omega t)$ with amplitude $\hat{j}_1=j_0-0.066$, frequencies $\omega=3.26$ (solid circles) and $\omega=6.51$ (open circles), and different mean values $j_0\approx 1$. Solid curves show the corresponding results of the Lorenz model with sidewall forcing ($f=0.005$). In the absence of sidewall forcing ($f=0$), the Lorenz model yields the short-dashed curve for $\omega=6.51$ and the dot-dashed curve for $\omega=3.26$. Dotted line shows the relation between $j_0^{\rm conv}$ and r_0 when modulation and sidewall forcing are absent ($f=\hat{j}_1=0$).

In a separate experiment, we obtained $j_0^{\rm conv}$ at constant $j_0=1.005$ and $\hat{j}_1=0.94$, for several ω. The data are shown as solid circles in Fig. 6 together with the theoretical predictions for three different values of f. The figure illustrates the sensitivity of the model in this region near $j_0=r_0=1$ to varying the mismatch parameter f. The best fit here also corresponds to $f=0.005$ (solid line) as in Fig. 5. This agreement in the frequency dependence is not automatic and can be considered a successful test of the model. As mentioned above, the value $f=0.0016$ obtained from previous experiments under very different conditions[10] and derived approximately from a theory of the sidewall forcing[11] would show a considerable deviation from the data.

It is of some interest to ask how important the frequency dependence of the function $\psi(\omega\nu)$ [see Appendix A and Fig. 13 below] is in obtaining the fit in Fig. 6. We have thus repeated the analysis setting $\psi(\omega)\equiv 1$ and obtained the results in Fig. 7. The ensuing fit is somewhat worse than before but the basic frequency dependence of $j_0^{\rm conv}$ is still correctly given. This is gratifying since the specific form of $\psi(\omega)$ depends sensitively on the Lorenz truncation and is thus on somewhat less firm footing than the other terms in ξ_ν, Eq. (4.3), which are also present in the exact low-frequency analysis of Cross *et al.*[11]

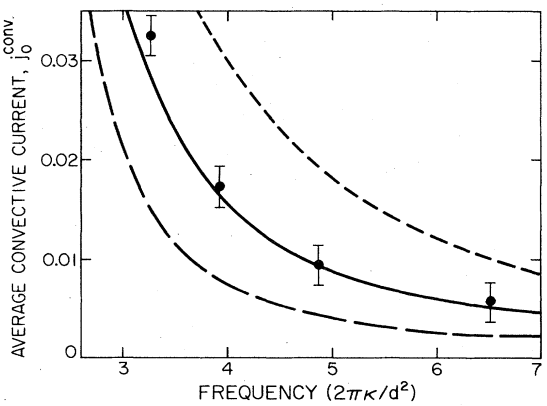

FIG. 6. Average convective current vs frequency for a total current $j(t)=1.005+0.94\sin(\omega t)$. Solid circles with error bars represent experimental data. Lines show the predictions of the Lorenz model in the presence of dynamical sidewall forcing of different strengths $f=0.005$ (solid line), 0.0025 (long dashes), and 0.0100 (short dashes).

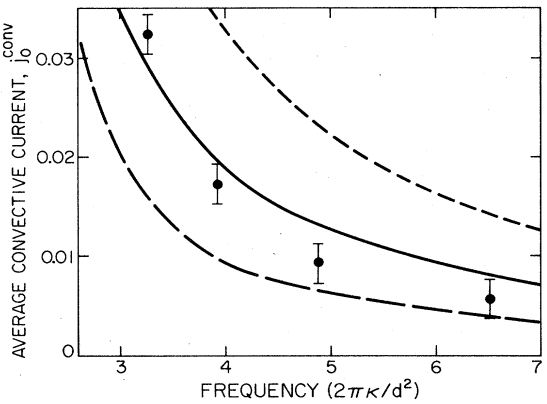

FIG. 7. Average convective current vs frequency for a total current $j(t)=1.005+0.94\sin(\omega t)$ as in Fig. 6 but with a simplified sidewall forcing [$\psi\equiv 1$ in Eq. (4.3)]. Solid circles represent experimental data and the lines show predictions of the Lorenz model in the presence of sidewall forcing of different strengths $f=0.005$ (solid line), 0.0025 (long dashes), and 0.010 (short dashes).

2. *Results above threshold*

An experiment was conducted at constant $\omega=6.51$ but for several $j_0\simeq\hat{j}_1\gtrsim 1$. It yielded the results shown as solid circles in Fig. 8 for the modulated case. For the same j_0 the unmodulated portion of the experiment gave the open circles. The arrows indicate the change in j_0^{conv} and r_0 when the modulation is turned on. It is seen from Fig. 8 that the constant-frequency experiment with the smallest value of r_0 shows an increase of convection, while modulation at larger values of r_0 depresses the convection in comparison with static driving. The fact that the unmodulated data (open circles) coincide with the solution of the model for static driving (dotted line) also implies that the sidewall forcing is negligible in the static case (see also Fig. 13 of BA). For the sake of completeness, we also show (dashed line) the theoretical prediction for the mean convective current in the presence of modulation, but for the ideal situation without dynamical sidewall forcing ($f=0$).

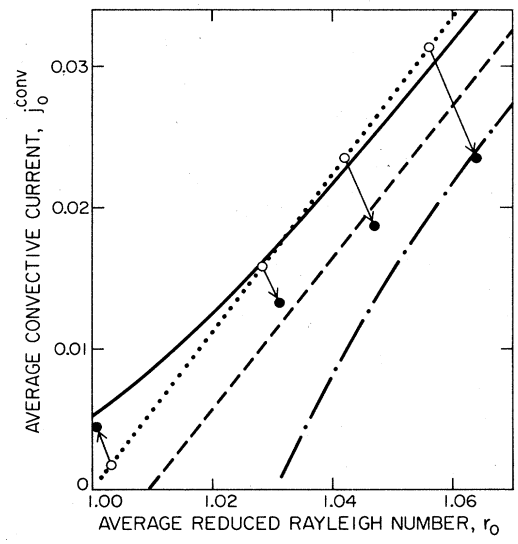

FIG. 8. Average convective current j_0^{conv} vs average reduced Rayleigh number r_0 resulting from a current $j(t)=j_0+\hat{j}_1\sin(\omega t)$ with $\omega=6.51$. Open circles show data in the absence of modulation ($\hat{j}_1=0$, $j_0\simeq 1$). Closed circles show data in the modulated case ($\hat{j}_1=j_0-0.066$). Mean current j_0 was the same for each data pair connected by an arrow but varied from pair to pair. Solid and dash-dotted lines show the predictions of the Lorenz model (4.1)–(4.5) and correspond to the two different periodic attractors with convection enhanced and depressed by dynamical sidewall forcing, respectively. In the absence of sidewall forcing ($f=0$), the Lorenz model yields the dashed line if the current is modulated ($\hat{j}_1\neq 0$) and the dotted line in the static case ($\hat{j}_1=0$).

If the sidewall forcing is included, the model has two different periodic solutions for a significant parameter range, i.e., two stable periodic attractors, as discussed in more detail in Sec. V C of I. Within the model, these solutions describe fluid flow in two opposite directions. Whereas for $f=0$ the physical properties of the solutions are the same, this degeneracy is lifted by the dynamical sidewall forcing. The mean convective currents corresponding to the two attractors are shown in Fig. 8 as solid and dot-dashed lines corresponding to enhanced and depressed convection, respectively. The suppressed convective state of the model (dot-dashed line), when it exists, evolves from suitable negative initial conditions for x and y with positive forcing f. The enhanced convective state (solid line), on the other hand, results from appropriate positive initial conditions for x and y.

For $r_0\lesssim 1.03$, only the upper branch exists and the left most data point, as well as some of those in Figs. 5 and 6, agree well with the calculation. The experimental result for the largest r_0 in Fig. 8 lies very close to the lower branch of the model, with suppressed convective currents. However, for the two intermediate values close to $r_0=1.04$, the agreement is not good with either branch; of course, it must be remembered that the differences are only a few tenths of one percent.

In addition to our constant-frequency experiment, we conducted two sequences each at constant j_0 and $\hat{j}_1$ but with varying ω. Here it is worth remembering that at constant j_0 and j_1 the size $|r_1|$ of the first Fourier coefficient of the temperature difference across the cell is strongly dependent upon ω. In the absence of convection, $|r_1|$ is equal to $|j_1\mathcal{P}(\omega)|$, and increasing ω from four to eight, for example, decreases $\mathcal{P}(\omega)$ by a factor of 2 [see Fig. 4(a)], with a corresponding change in the value of $|r_1|$.

In order to minimize the effect of long-term experimental drift upon the results, we find it best to examine the difference in the mean convective current in the presence and absence of modulation. In Fig. 9(a) ($j_0=1.066$, $\hat{j}_1=1.000$) and Fig. 9(b) ($j_0=1.301$, $\hat{j}_1=1.235$), we show by dots the experimental data[19] for $j_0^{conv}-j_{stat}^{conv}$, i.e., for the excess convective current averaged over one cycle relative to its value j_{stat}^{conv} under static driving with the same applied current j_0. The corresponding j_{stat}^{conv} was obtained during the time intervals of steady heating separating the segments with the different modulation frequencies indi-

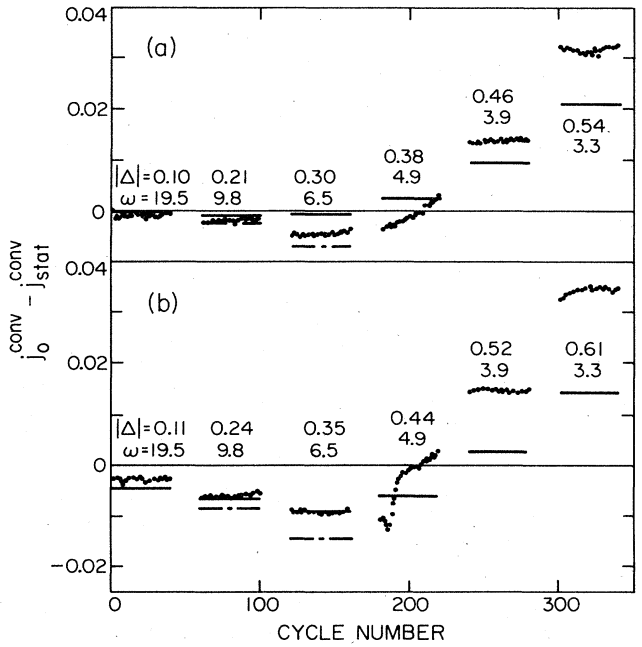

FIG. 9. Excess convective current averaged over one modulation cycle vs cycle number. Dots show the measured change of the average convective current induced by modulation with a fixed mean current (a) $j_0=1.066$, (b) $j_0=1.301$. Modulation amplitude $\hat{j}_1$ was (a) 1.000 and (b) 1.235. The relative amplitude $|\Delta|=2|r_1|/r_0$ of the temperature difference increases from left to right as the modulation frequency ω decreases. Intervals with static heating between data segments are not shown at their full length. Corresponding results of the Lorenz model for the periodic attractors with enhanced and suppressed convection are shown (as far as they exist) by solid and dot-dashed horizontal bars, respectively. They correspond to the solid and dot-dashed lines in Fig. 8.

cated in Fig. 9. The data points, one for each cycle and 40 within each frequency segment, are shown as a function of cycle number, thus retaining the time sequence in which they were taken but distorting the time scale of the abcissa since the period increases from segment to segment as we move from left to right. Furthermore, the time intervals between the data segments where the heating was unmodulated are not shown at their full length. The values of Δ and ω identifying each data segment are included in Fig. 9.

The first three segments correspond to stationary periodic states for which modulation inhibits convection, i.e., $j_0^{conv} < j_{stat}^{conv}$. The fourth segment in each case, but most dramatically in Fig. 9(b), shows transient behavior which we attribute to the process of switching from one attractor (which is either unstable or has ceased to exist at this point) to the other. The solid and dot-dashed horizontal bars in the figures are the model predictions for the attractors with enhanced and depressed convective current, respectively. They correspond to the solid and dot-dashed lines in Fig. 8. As stated before, the agreement between experiment and theory is only semiquantitative, especially at low frequencies, but the limit of existence at large Δ (small ω) of the attractor with the depressed convective current coincides extremely well with the experimentally observed transient behavior.

In Fig. 10(a) ($j_0=1.066$, $\hat{j}_1=1.000$) and Fig. 10(b) ($j_0=1.301$, $\hat{j}_1=1.235$), we summarize the information on the mean excess convective current, $j_0^{conv}-j_{stat}^{conv}$, contained in Figs. 9(a) and 9(b). Points denote averages over the 40 cycles contained in each data segment displayed in Fig. 9. The thick vertical bars at $\omega=4.9$ correspond to the transient cases. They extend from the smallest to the largest value observed at the corresponding current and frequency. The solid and dot-dashed lines are theoretical results for the solutions with enhanced and suppressed current, respectively, as in Figs. 8 and 9. The arrows indicate the limits of existence in the model of the attractor with the low convective current. For large ω (small Δ) the data provide evidence for inhibition of convection by modulation which is of the same magnitude as that found in the model. The switching in the experiment from the low to the high current branch occurs almost precisely at the value of ω (and Δ) at which the suppressed-current attrac-

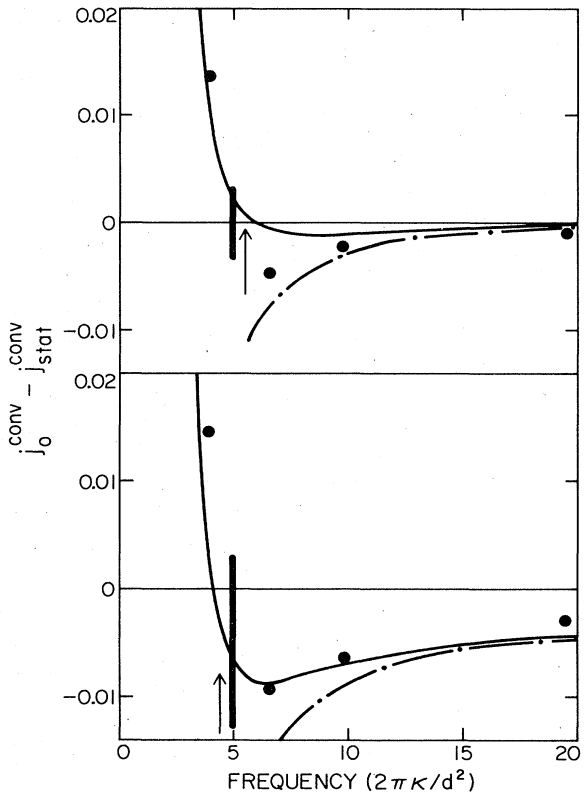

FIG. 10. Mean excess convective current vs modulation frequency [j_0 and $\hat{j}_1$ as in Figs. 9(a) and 9(b)]. Solid circles denote average over the 40 cycles in each data segment of Fig. 9. Thick vertical bars at $\omega=4.9$ extend from the smallest to the largest value observed in the transition (cf. Fig. 9) from a state with $j_0^{conv} < j_{stat}^{conv}$ to one with $j_0^{conv} > j_{stat}^{conv}$. Solid and dash-dotted lines are the theoretical results for the attractors with enhanced and suppressed convection, respectively, as in Figs. 8 and 9. When the latter attractor ceases to exist, the model predicts a transition (marked by arrows) to the former.

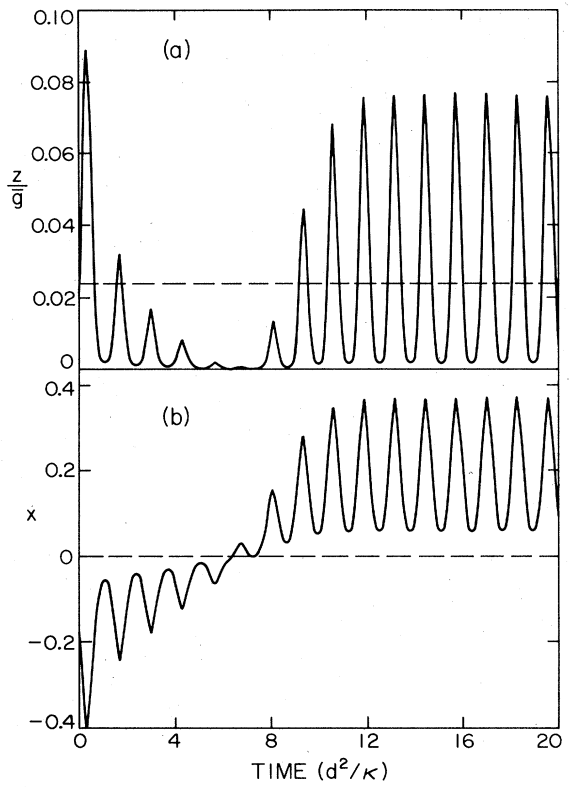

FIG. 11. Lorenz-model calculation of the transition to the periodic attractor with enhanced convection for $r_0=1.0425$, $r_1=0.175$ ($\Delta=0.336$), $\omega=4.885$, and $\sigma=0.78$. Quantities shown are (a) $j^{\rm conv}(t)=z(t)/\bar{g}$ and (b) $x(t)$. Dashed line in (a) corresponds to $j^{\rm conv}_{\rm stat}=z_{\rm stat}/\bar{g}$ with $\bar{g}=1.78$. At time $t=0$, the system starts near the solution with suppressed convection (see Fig. 8), but the parameters are such that this solution no longer corresponds to a stable periodic attractor, so the system makes a transition to the periodic solution with enhanced convection.

tor of the model (which is occupied at large ω) ceases to exist. We regard this switching phenomenon in the data to be a dramatic confirmation of the applicability of the model to the real system.

Finally, in Fig. 11, we show an example of the transients associated with the switching as calculated from the model. In Fig. 11(a), we display the evolution of $z(t)/\bar{g}$, which is analogous to the experimental $j^{\rm conv}(t)$. Figure 11(b) shows $x(t)$ (y behaves similarly). The results were obtained by starting the integration with negative initial conditions for x and y. The attractor corresponding to a negative x and y no longer exists for the value of ω and Δ used in the calculation, and, after a number of cycles, the system finds the only existing attractor, corresponding to positive x and y. This phenomenon is qualitatively similar to that observed in the real system, although the time scale of the transition is somewhat different.

B. Time dependence

So far we have compared only the mean value r_0 of $r(t)$ with the predictions of the model. A great deal of

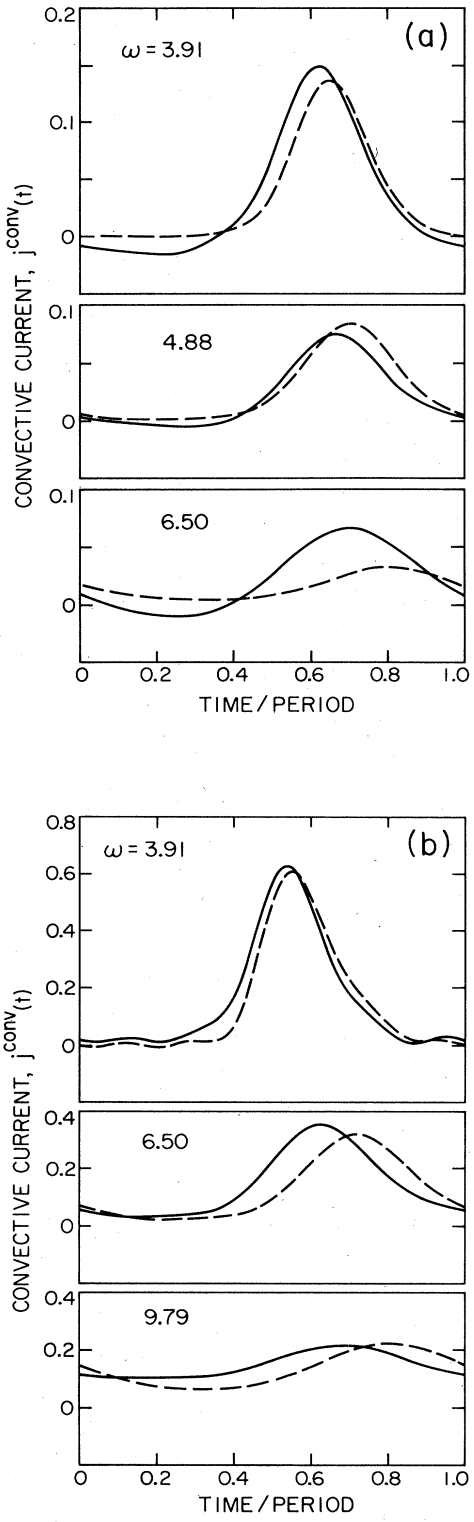

FIG. 12. Time dependence of the convective current over one period. Solid lines are the experiment and dashed lines the corresponding results from the Lorenz model. Total current applied at the lower plate was $j(t)=j_0+\hat{j}_1\sin(\omega t)$, with (a) $j_0=1.066$ and $\hat{j}_1=1.000$ and (b) $j_0=1.301$ and $\hat{j}_1=1.235$.

TABLE II. Amplitudes and phases of the Fourier coefficients $r_\nu = |r_\nu| \exp(i\phi_\nu)$ of the Rayleigh number for various modulation frequencies ω. (a) The current applied to the lower plate is $j(t) = 1.066 + 1.000 \sin(\omega t)$. For this case $\bar{g} = 1.78$. (b) The current to the lower plate is $j(t) = 1.301 + 1.235 \sin(\omega t)$. For this case $\bar{g} = 1.20$.

	ω	r_0	$\lvert r_1 \rvert$	ϕ_1	$10^3 \lvert r_2 \rvert$	ϕ_2	$10^3 \lvert r_3 \rvert$	ϕ_3	$10^3 \lvert r_4 \rvert$	ϕ_4	$10^3 \lvert r_5 \rvert$	ϕ_5
						(a)						
Expt.	19.57	1.038	0.0529	3.71								
Theor.	19.57	1.042	0.0525	3.70								
Expt.	9.79	1.044	0.1095	3.20								
Theor.	9.79	1.045	0.1102	3.21								
Expt.	6.50	1.046	0.1565	2.98	0.55	1.0	0.03	−0.4				
Theor.	6.50	1.051	0.1528	2.99	0.27	2.5	0.03	1.6				
Expt.	4.88[a]	1.044	0.1985	2.83	1.6	0.5	0.015	2.4	0.06	3.0		
Theor.	4.88[b]	1.040	0.1992	2.83	1.7	1.0	0.35	5.7	0.06	3.9		
Expt.	3.91	1.028	0.2375	2.70	4.0	−1.0	1.08	4.0	0.30	1.7	0.05	5.1
Theor.	3.91[b]	1.032	0.2362	2.71	3.9	0.3	1.20	4.6	0.30	2.4	0.08	6.4
						(b)						
Expt.	19.57	1.150	0.0654	3.71								
Theor.	19.57	1.164	0.0648	3.71								
Expt.	9.79	1.160	0.1405	3.18	0.72	1.2						
Theor.	9.79	1.168	0.1434	3.22	0.68	2.8						
Expt.	6.50	1.164	0.2042	2.92	4.26	0.3	0.8	4.3				
Theor.	6.50	1.175	0.2075	2.97	3.86	1.4	0.7	6.0				
Expt.	4.88[a]	1.158	0.2580	2.74	10.1	−0.4	2.8	3.5	0.8	0.8		
Theor.	4.88	1.205	0.2639	2.81	8.2	0.8	2.3	5.2	0.7	3.1		
Expt.	3.91	1.140	0.2995	2.58	17.3	5.2	5.6	2.5	2.0	5.9	1.0	3.2
Theor.	3.91[b]	1.159	0.3084	2.71	17.1	5.6	6.1	2.8	2.2	6.1	1.0	3.1

[a]Transient.
[b]After switching attractors.

additional information is contained in the higher Fourier components r_ν, $\nu > 0$. In Table II we compare the magnitude $|r_\nu|$ and the phase ϕ_ν of r_ν with the model predictions for the two experimental sequences at constant $j_0, \hat{j}_1$ and varying ω (and thus Δ), which were already considered in Figs. 9 and 10. We have included all Fourier components which were significantly larger than the experimental background and for which $\omega\nu \leq 19.57$ [for larger $\omega\nu$ the transfer function $\mathscr{P}(\omega\nu)$ had not been measured and a comparison is thus not possible]. It is worth noting that the values of r_0, $|r_1|$, and ϕ_1 are determined primarily by the conductive current. Their values will thus be close to the theoretical prediction if the transfer function $\mathscr{P}(\omega\nu)$ is known well enough. On the other hand, the applied current contained only $\nu = 0$ and $\nu = 1$ components, and thus the *entire* values of $|r_\nu|$ and ϕ_ν for $\nu \geq 2$ are determined by the nonlinear convective process. Thus it is gratifying that the experimental amplitudes for $\nu \geq 2$ are generally within 20% or so of the model predictions. The phases are typically within one or two radians. We believe that this comparison of the high Fourier components provides a nontrivial test of the validity of the mode truncation inherent in the model for the parameter range of the present experiments.

An alternative way of comparing the finite-frequency response of the real system with the model is to reconstruct the convective current $j^{\text{conv}}(t)$ from the measured $r(t)$. We do this by subtracting the conductive current $j^{\text{cond}}(t)$, obtained from its components $j_\nu^{\text{cond}} = r_\nu / \mathscr{P}(\omega\nu)$, from the total current $j(t)$ [cf. Eq. (4.5)]. The result is compared in Fig. 12 with the model prediction $j^{\text{conv}}(t) = z(t)/\bar{g}$ for the two experimental sequences. A similar comparison for one of them [Fig. 12(b)] was shown already in Fig. 2 of Ref. 15, but it was based on a slightly different theoretical model. The change in the model has had only very little influence on the relationship between the experimental and theoretical results. When looking at the comparison in Fig. 12, one should consider that j^{conv} is dominated by the contribution from j_1^{conv}. Any small discrepancy between theory and experiment for $r(t)$ is therefore greatly magnified in j^{conv} because j_1^{conv} is the small difference between j_1 and $r_1/\mathscr{P}$, both of which are of order unity in our experiment. The agreement between theory and experiment in the wave shape of $j^{\text{conv}}(t)$ is clearly quite good, except perhaps for the case $\omega = 6.5$ in Fig. 12(a). The discrepancy seen there comes primarily from the small differences between experiment and theory for $|r_1|$ and $|r_2|$ which can be found in Table II(a) for $\omega = 6.50$.

VI. CONCLUSION

We conclude by discussing possible future experiments designed to test our model in more detail and to explore a broader range of physical parameters. The most basic qualitative test of the model involves flow visualization techniques to verify the assumption that the roll state persists under modulation. As mentioned in the Introduc-

tion, this assumption is not generally correct in a laterally infinite system,[12] so its justification depends on the existence of the sidewall forcing. A preliminary experiment by Steinberg *et al.*[13] has shown that under conditions similar to the ones of the experiments reported here, the pattern does remain roll-like in the presence of modulation. Presumably, as the sidewall forcing becomes weaker, either by increasing the aspect ratio or by appropriate thermal matching of the sidewalls and the fluid, the convective pattern will begin to show the predicted hexagonal behavior of the ideal system. In any case, it is important to understand more precisely, both from experiment and from theory, under what conditions one or the other pattern will be seen.

Another desirable extension of the experiments is toward larger values of the modulation amplitude Δ. This can most conveniently be achieved by controlling the temperature of the plates directly, rather than the heat current. With values of Δ on the order of 1–3 (rather than $\Delta \lesssim 0.6$), one can hope to test more of the predictions made in I. Examples are the threshold shift due to modulation, the onset of convection at twice the driving period for $\Delta \gtrsim 2$, and the variation with Δ of the initial slope of the mean convective current versus Rayleigh number. Of course, for all of the above properties, which involve the behavior near threshold, it is important to minimize the sidewall forcing, since the properties in question are those of the ideal system. With judicious choices of materials and of geometry, it seems likely that one will be able to reduce the sidewall forcing by at least an order of magnitude.

Finally, we may mention the possibility of more advanced experiments involving modulation with two or more frequencies,[20] or modulation of more complicated systems such as fluid mixtures near higher-codimension bifurcations[21] where periodic modulation might induce nonperiodic response even near the convective threshold.[22] In all of these cases, external control of some of the fluid variables provides a convenient probe to study the dynamical behavior of the system.

ACKNOWLEDGMENTS

The authors are indebted to M. C. Cross for valuable discussions and to R. P. Behringer for building the apparatus in which the measurements were made. A portion of this work was carried out while two of us (P.C.H. and M.L.) were at the Institute for Theoretical Physics at the University of California, Santa Barbara. The research was supported by the National Science Foundation (NSF) under Grants No. MEA-81-17241 and No. PHY-77-27084 and by the North Atlantic Treaty Organization (NATO) under Grant No. 128.82.

APPENDIX A: THE SIDEWALL FORCING FUNCTION

In Appendix D of I we derived the sidewall forcing $\xi(t)$, which couples to the (1,0,1) velocity mode retained in the Lorenz model. The calculation was performed for stress-free horizontal boundaries, but the general form of the result should be the same for the rigid case. The forcing function was written in the form

$$\xi(t)=\sqrt{3}\pi\hat{S}_w(1,0,1;t)/R_c^{\rm stat} . \tag{A1}$$

The physical origin of this forcing is that in the presence of modulation the sidewalls generate "heat waves" entering the fluid laterally and thereby induce convective flow. For stress-free horizontal boundaries the frequency Fourier components of the forcing function $\hat{S}_w$ are

$$\frac{S_\nu^w(1,0,1)}{R_c^{\rm stat}}=i\omega\nu r_\nu \frac{(\pi/\sqrt{2})\sin(\pi L/\sqrt{2})+\Omega_\nu\cos(\pi L/\sqrt{2})\tanh(\Omega_\nu L)}{\pi L\,\Omega_\nu^2(\Omega_\nu^2+\pi^2/2)}\phi_\nu , \tag{A2}$$

with

$$\phi_\nu=(1-\lambda_1)\frac{\pi^2}{\bar{\Omega}_\nu^2}\left[1+\lambda_2\frac{\Omega_\nu}{\bar{\Omega}_\nu}\frac{\tanh(\Omega_\nu L)}{\tanh(\bar{\Omega}_\nu t_w)}\right]^{-1} , \tag{A3}$$

$$\Omega_\nu^2=\pi^2-i\omega\nu,\quad \bar{\Omega}_\nu^2=\pi^2-i\omega\nu\lambda_1 . \tag{A4}$$

Here

$$\lambda_1=\kappa_f/\kappa_w,\quad \lambda_2=K_f/K_w \tag{A5}$$

denote ratios of thermal diffusivities and conductivities, respectively, of the fluid and the sidewalls (for our cell $\lambda_1=6\times10^{-4}$, $\lambda_2=0.17$). The lateral width of the fluid layer is $2L$ ($2L=D/d=9.44$) and the wall thickness is denoted by t_w ($t_w=0.058$).

For the geometry of our cell and our modulation frequencies, (A2) and (A3) simplify somewhat: since $\mathrm{Re}(\Omega_\nu L)\gg1$, we may replace $\tanh(\Omega_\nu L)$ by 1. Furthermore, since λ_1 is so small that $\omega\nu\lambda_1/\pi^2\ll1$ for all our modulation frequencies and Fourier indices ν, we obtain $\tanh(\bar{\Omega}_\nu t_w)\simeq\tanh(\pi t_w)$ which itself may be replaced by πt_w because of the small wall thickness t_w. Therefore, ϕ_ν simplifies in our system to

$$\phi_\nu\simeq(1-\lambda_1)(1+\lambda_2\Omega_\nu/\pi^2 t_w)^{-1} . \tag{A6}$$

Then the Fourier coefficients ξ_ν of the forcing function are given by

$$\xi_\nu=i\omega\nu r_\nu\tilde{\psi}(\omega\nu) , \tag{A7}$$

$$\tilde{\psi}(\omega\nu)=\frac{\sqrt{3}}{L}\frac{(\pi/\sqrt{2})\sin(\pi L/\sqrt{2})+\Omega_\nu\cos(\pi L/\sqrt{2})}{\Omega_\nu^2(\Omega_\nu^2+\pi^2/2)}\times\left[1+\frac{\lambda_2\Omega_\nu}{\pi^2 t_w}\right]^{-1} . \tag{A8}$$

In I we have defined the mismatch parameter

$$f=\tilde{\psi}(0)\ , \tag{A9a}$$

which may be rewritten as

$$f=\sqrt{2}(1-\lambda_1)(\cos\alpha)[\pi^3 L(1+\lambda_2/\pi t_w)]^{-1}\ , \tag{A9b}$$

in terms of the phase angle

$$\alpha=\pi L/\sqrt{2}-\cot^{-1}(\sqrt{2})\ . \tag{A9c}$$

Then ξ_ν may be expressed in the form

$$\xi_\nu=i\omega\nu r_w f\psi(\omega\nu) \tag{A10}$$

with

$$\psi(\omega\nu)=\tilde{\psi}(\omega\nu)/\tilde{\psi}(0)\ . \tag{A11}$$

The factor $\cos\alpha$ in (A9b) depends sensitively on the assumed roll pattern and is not to be considered as reliably calculated. In any case, in this work we determined f experimentally and used (A10) as the forcing function with $\psi(\omega\nu)$ [Eq. (A11)] being determined by (A8) and (A11). In Fig. 13 we show the amplitude and phase of $\psi(\omega)$ for the parameters of our system.

Lastly, we mention that ξ_ν [Eq. (A10)] generalizes to the formula

$$\xi_\nu=i\omega\nu(T_\nu^l+T_\nu^u)(R_c^{\rm stat})^{-1}f\psi(\omega\nu) \tag{A12}$$

given in Eq. (5.3) of I when the temperature T^u of the upper plate also varies in time.

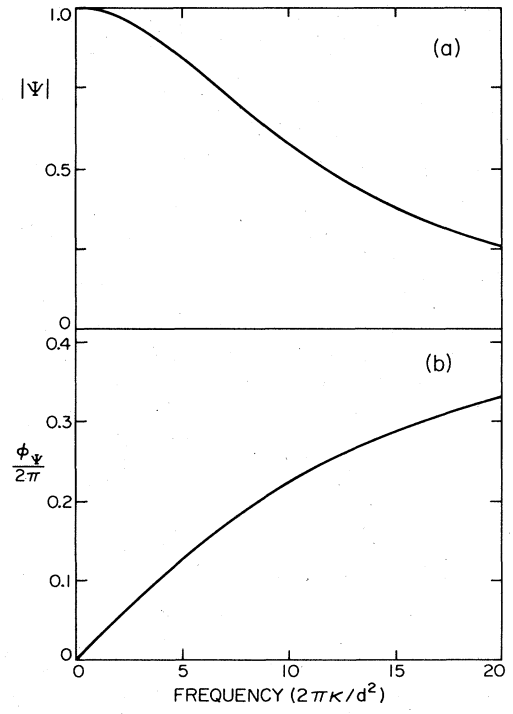

FIG. 13. Amplitude and phase of the function $\psi(\omega)$ defined in Eqs. (A2)—(A6). This function contributes to the frequency dependence of the sidewall forcing $\xi(\omega)$.

APPENDIX B: THE CONDUCTIVE TRANSFER FUNCTION

Here we evaluate the conductive transfer function for a laterally infinite system consisting of a fluid layer above a solid lower plate of thickness d_l as shown schematically in Fig. 14. For such a system, Behringer *et al.*[23] have determined the relation between the temperature in the fluid at $x_3=0$ (i.e., at the top of the lower plate) and that at $x_3=-d_l$ (i.e., at the bottom of the lower plate) when the heat flux at $x_3=-d_l$ is constant. For the situation with fixed temperature at $x_3=-d$, they compared the current entering the fluid at $x_3=0$ with that entering the bottom plate at $x_3=-d_l$. Here we let the temperatures at the top of the fluid,

$$T(x_3=1,t)=T^u(t)\ , \tag{B1}$$

and at the *bottom* of the lower plate,

$$T(x_3=-d_l,t)=T^l(t)\ , \tag{B2}$$

be periodic in time with period $2\pi/\omega$. Then the conductive temperature profile is periodic as well,

$$T(x_3,t)=\sum_{\nu=-\infty}^{\infty}T_\nu(x_3)e^{-i\omega\nu t}\ , \tag{B3}$$

and its spatial dependence is determined in both media by a sum of two exponentials

$$T_\nu(x_3)=\begin{cases}A_\nu e^{iq_\nu x_3}+B_\nu e^{-iq_\nu x_3}, & 0<x_3\le 1\\ A_\nu^l e^{iq_\nu^l x_3}+B_\nu e^{-iq_\nu^l x_3}, & -d_l\le x_3\le 0\ .\end{cases} \tag{B4}$$

Here

$$q_\nu=(i\omega\nu)^{1/2},\quad q_\nu^l=q_\nu(\kappa_f/\kappa_l)^{1/2}\ , \tag{B5}$$

where κ_f and κ_l are the thermal diffusivities of the fluid and the lower plate, respectively. The four amplitudes entering (B4) are determined by the temperatures (B1) and (B2) and the fact that the temperature and the heat current must be continuous at the interface $x_3=0$. A straightforward calculation then yields the Fourier amplitudes $j_\nu^{\rm cond}$ of the conductive current at the bottom of the lower plate, as a function of the amplitudes T_ν^l and T_ν^u of the temperatures at $x_3=-d_l$ and $x_3=1$, respectively:

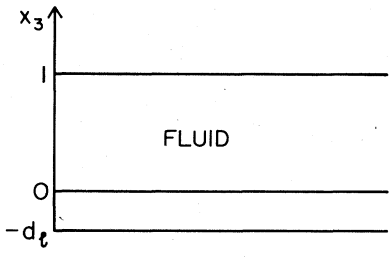

FIG. 14. Schematic diagram showing the fluid of depth $d_f=1$ and the lower plate of thickness d_l.

$$j_\nu^{\rm cond} R_c^{\rm stat} = \left[T_\nu^l \left[1 - \frac{\lambda_3}{\lambda_4} \tan(q_\nu) \tan(\lambda_3 \lambda_4 q_\nu) \right] - T_\nu^u \frac{1}{\cos(q_\nu)\cos(\lambda_3\lambda_4 q_\nu)} \right] \frac{\lambda_3(1+\lambda_4^2) q_\nu}{\lambda_3 \tan(q_\nu) + \lambda_4 \tan(\lambda_3\lambda_4 q_\nu)} \ . \tag{B6}$$

Here we introduced the constants

$$\lambda_3^2 = d_l \rho_l c_l / \rho_f c_f \tag{B7}$$

for the ratio of thermal masses of the lower plate and of the fluid (ρ denotes the density and c the specific heat), and

$$\lambda_4^2 = d_l K_f / K_l \ , \tag{B8}$$

which is determined by the ratio of the thermal conductivities ($K = \rho c \kappa$) of the fluid and the lower plate.

The reduced current $j^{\rm cond}(t)$ and the reduced vertical temperature difference $r(t)$ across the system are normalized such that their averages are equal [see Eq. (2.13)],

$$j_0^{\rm cond} = r_0 \ . \tag{B9}$$

Higher Fourier amplitudes $j_\nu^{\rm cond}$ depend in general not only on the temperature difference but on T_ν^l and T_ν^u separately. If, however, the temperature at the upper fluid surface is constant, i.e.,

$$T_\nu^u = T^u \delta_{\nu,0} \ , \tag{B10}$$

as in our experimental setup, then the quotient

$$\frac{j_\nu^{\rm cond}}{r_\nu} \equiv \frac{1}{\mathscr{P}(\omega\nu)} = \frac{\lambda_3(1+\lambda_4^2) q_\nu}{\lambda_3 \tan(q_\nu) + \lambda_4 \tan(\lambda_3\lambda_4 q_\nu)} \times \left[1 - \frac{\lambda_3}{\lambda_4} \tan(q_\nu) \tan(\lambda_3\lambda_4 q_\nu) \right] \tag{B11}$$

is temperature independent, and thus gives the inverse of the conductive heat transfer function of the idealized system.

In the limit $\lambda_4 \to 0$ where the conductivity of the lower plate is much larger than that of the fluid, the formula for $\mathscr{P}$ simplifies [as in Eq. (4.4)]:

$$\mathscr{P}(\omega\nu) = \frac{\tan(q_\nu)/q_\nu}{1 - \lambda_3^2 q_\nu \tan(q_\nu)} \ . \tag{B12}$$

Both formulas (B11) and (B12) have been compared with the experimentally determined transfer function of our system as discussed in Sec. IV C.

APPENDIX C: ITERATIVE INVERSION OF THE MODEL

In this appendix we discuss in more detail the iterative procedure used to solve Eqs. (4.5) for $r(t)$ subject to the condition that the total current $j(t)$ is given. Our solution method consists of the following steps. (i) Integration of the model differential equations (4.1) to obtain $z(t)$ with an initial $r(t)$ which is specified below. The integrations were performed using a fourth-order Runge-Kutta procedure. The initial conditions were taken in general to be the fixed-point solutions in the absence of modulation. The time steps for the integration were $\Delta t < \min\{0.02, \pi/16\omega\}$. (ii) Fourier analysis of $z(t)$ to determine the coefficients z_ν. This was done with a fast Fourier transform. The first several cycles of $z(t)$ were discarded to avoid transients. (iii) Evaluation of the temperature Fourier coefficients according to Eq. (4.5b):

$$r_\nu = (j_\nu - z_\nu/\bar{g}) \mathscr{P}(\omega\nu) \ . \tag{C1}$$

These coefficients determine the function $r(t)$. The result (C1) was used as input for (i) when it was necessary to perform another iteration of steps (i)—(iii).

The iteration could be started with the approximation that the total imposed current $j(t)$ is carried by conduction alone, i.e., $z^{(0)}(t) = 0$, so that the Fourier coefficients of $r^{(0)}(t)$ in step (i) would be $r_\nu^{(0)} = j_\nu \mathscr{P}(\omega\nu)$. Then steps (i)—(iii) give $r^{(1)}(t)$, and so on. A starting approximation which is somewhat better than neglecting convection altogether (by setting $z_\nu^{(0)} = 0$), is to use for the convective current the stationary value it would have in the absence of modulation, i.e.,

TABLE III. Amplitudes and phases of the Fourier coefficients $r_\nu = |r_\nu| \exp(i\phi_\nu)$ occurring in the iterative solution of Eqs. (4.5) starting with $r_0^{(0)} = (\bar{g} j_0 + 1)/(1+\bar{g})$, $r_1^{(0)} = j_1(\omega)\mathscr{P}(\omega)$. The parameters were $\bar{g} = 1.78$, $j_0 = 1.0657$, $|j_1| = \hat{j}_1/2 = 0.500$.

Iteration	r_0	$\lvert r_1 \rvert$	ϕ_1	$10^4 \lvert r_2 \rvert$	ϕ_2
		$\omega = 9.77$			
0	1.0425	0.2190	3.200	0	
1	1.0435	0.2213	3.206	1.6	3.19
4	1.0431	0.2213	3.206	1.7	3.20
10	1.0431	0.2213	3.206	1.7	3.20
		$\omega = 3.91$			
0	1.0425	0.4519	2.743	0	
1	1.0302	0.4735	2.715	77.1	0.353
4	1.0320	0.4725	2.714	78.2	0.311
10	1.0320	0.4725	2.714	78.3	0.310

$$z_0^{(0)}/\bar{g}=(j_0-1)/(1+\bar{g});\quad z_\nu^{(0)}=0 \text{ for } |\nu|\geq 1\ . \tag{C2a}$$

Then

$$r_\nu^{(0)}=(j_\nu-z_\nu^{(0)}/\bar{g})\mathscr{P}(\omega\nu) \tag{C2b}$$

is the initial input for step (i).

We found that both starting approximations led to the same $r(t)$, with the second procedure converging slightly more rapidly. Some typical results, using the second procedure, are given in Table III for the first, fourth, and tenth iteration. In this case it is apparent that four iterations are sufficiently close to the final answer for comparison with experiment, but in general we used the results of ten iterations since we found this to be necessary in some cases.

[1]G. Ahlers, P. C. Hohenberg, and M. Lücke, preceding paper, Phys. Rev. A **32**, 3493 (1985). Referred to as paper I.

[2]R. J. Donnelly, F. Reif, and H. Suhl, Phys. Rev. Lett. **9**, 363 (1962).

[3]R. J. Donnelly, Proc. R. Soc. London Ser. A **281**, 130 (1964).

[4]S. H. Davis, Annu. Rev. Fluid Mech. **8**, 57 (1976).

[5]R. G. Finucane and R. E. Kelly, Int. J. Heat Mass Transfer **19**, 71 (1976).

[6]J. P. Gollub and S. V. Benson, Phys. Rev. Lett. **41**, 948 (1978).

[7]A. Oberbeck, Ann. Phys. Chem. **7**, 271 (1879); J. Boussinesq, *Theorie Analytique de la Chaleur* (Gauthier-Villars, Paris, 1903), Vol. 2.

[8]C. Normand, Y. Pomeau, and M. G. Velarde, Rev. Mod. Phys. **49**, 581 (1977).

[9]E. N. Lorenz, J. Atmos. Sci. **20**, 130 (1963).

[10]G. Ahlers, M. C. Cross, P. C. Hohenberg, and S. Safran, J. Fluid Mech. **110**, 297 (1981).

[11]M. C. Cross, P. C. Hohenberg, and M. Lücke, J. Fluid Mech. **136**, 269 (1983).

[12]M. N. Roppo, S. H. Davis, and S. Rosenblat, Phys. Fluids **27**, 796 (1984).

[13]V. Steinberg, G. Ahlers, and D. S. Cannell (unpublished).

[14]G. Ahlers, P. C. Hohenberg, and M. Lücke, Bull. Am. Phys. Soc. **26**, 1271 (1981).

[15]G. Ahlers, P. C. Hohenberg, and M. Lücke, Phys. Rev. Lett. **53**, 48 (1984). In this work we introduced a Lorenz model in which the effects of rigid horizontal boundary conditions were treated in a purely phenomenological manner. Although there is very little quantitative difference between the two models, the present one is more satisfactory from a logical point of view since it is derived from the Oberbeck-Boussinesq equations with rigid boundary conditions. Note that the value $f=0.04$ quoted in Fig. 1 of the letter was the value of $\bar{f}'$. The corresponding value for f is 4.5×10^{-3} which is close to the value $f=5\times10^{-3}$ obtained in the present work.

[16]R. P. Behringer and G. Ahlers, J. Fluid Mech. **125**, 219 (1982). Referred to as BA.

[17]H. vanDijk, M. Durieux, J. R. Clement, and J. K. Logan, *The 1958 ^{4}He Scale of Temperature,* Natl. Bur. Stand. (U.S.) Monograph No. 10 (U.S. GPO, Washington, D.C., 1960).

[18]R. W. Walden and G. Ahlers, J. Fluid Mech. **109**, 89 (1981).

[19]We would like to mention that the mean excess convective current due to modulation of the current around j_0 is directly measurable: if one subtracts the identity (2.13) for static driving ($\hat{j}_1=0$) from that for modulated driving ($\hat{j}_1\neq0$), one finds (the total j_0 is the same in both cases) $j_0^{\rm conv}(\hat{j}_1)-\hat{j}_0^{\rm conv}(\hat{j}_1=0)=r_0(\hat{j}_1=0)-r(\hat{j}_1)=(T_{\rm stat}^l-T_0^l)/\Delta T_c^{\rm stat}$.

[20]M. Lücke and F. Schank, Phys. Rev. Lett. **54**, 1465 (1985).

[21]H. R. Brand, P. C. Hohenberg, and V. Steinberg, Phys. Rev. A **27**, 593 (1983); **30**, 2548 (1984).

[22]B. J. A. Zielinska, D. Mukamel, V. Steinberg, and S. Fishman, Phys. Rev. A **32**, 702 (1985).

[23]R. P. Behringer, C. Agosta, J. S. Jan, and J. N. Schaumeyer, Phys. Lett. **80A**, 273 (1980).